AN ANALYSIS OF THE DYNAMIC SHEAR FAILURE RESISTANCE OF STRUCTURAL METALS

K. MINNAAR AND M. ZHOU*

The George Woodruff School of Mechanical Engineering, Georgia Institute of Technology, Atlanta, GA 30332-0405, U.S.A.

ABSTRACT

The localization of shear deformation and the eventual rupture inside shear bands are analyzed experimentally. The shear failure resistance of several structural metals is compared. The materials studied are HY-80, HY-100, HSLA-80, 4340VAR, and Ti-6Al-4V. The evaluation of failure progression focuses on the evolution of both the stress-carrying capacities and material microstructures. Experiments show that despite its significantly stronger rate sensitivity, Ti-6Al-4V is more susceptible to shear localization and rupture compared with the steels, as demonstrated by its relatively early and precipitous loss of stress-carrying capacity. This observation is supported by measurements of the shear band and rupture lengths in specimens deformed to various stages of failure development. Among the steels, the martensitic micro-structure of HY-100 seems to be responsible for its higher susceptibility to localization. While all the steels studied show very similar dynamic constitutive responses, their significantly different shear failure behaviors suggest that macroscopic thermal-mechanical descriptions alone are not sufficient to account for the shear failure in the form of combined localization of strain and the eventual rupture through the shear bands. Consequently, microstructural damage mechanisms should also be considered. © 1998 Elsevier Science Ltd. All rights reserved.

Keywords: A. strain localization, B. viscoplastic material, ductile failure, C. Kolsky bar.

1. INTRODUCTION

Shear band formation rather than crack initiation is the principal form of failure for many structural metals under certain dynamic loading conditions. In most applications, this form of failure should be avoided. It is necessary to evaluate the resistance of similar materials to dynamic shear failure in order to achieve maximum structural integrity through design, materials selection and development of more advanced materials. Identifying the factors that determine the susceptibility or resistance of materials to the initiation and propagation of localized shear deformation has clear practical significance. Just as *fracture toughness* is a measure of material resistance to cracking, there may also be a toughness measure for material resistance to dynamic shear banding. Although the influences of many individual material properties on shear banding, such as strain hardening and rate sensitivity, are understood, no well-developed criterion is available for the comparison of the relative susceptibilities to shear localization of different materials. The difficulty arises partly because different

* To whom correspondence should be addressed. Fax: 001 404-894 8336.

materials have different combinations of properties. The lack of a criterion for the comparison of the relative resistance to shear failure is an issue in the design of structures and the selection of materials.

The occurrence of shear bands at high strain rates is a thermomechanical process driven mainly by heat due to plastic dissipation. Analyses of this phenomenon have either followed mechanics approaches, which are based on descriptions of the thermomechanical response of materials, or materials approaches, which focus on the microscopic evolution associated with the shear band development. The mechanics analyses have yielded understandings on the conditions for the onset and development of shear bands. For example, Clifton (1980) analyzed the effects of heat conduction and strain rate on the growth of perturbations in deformation fields. Molinari and Clifton (1987) obtained the critical condition for shear localization in closed form for several idealized models of simple shearing deformation. A sample of related work includes Rogers (1979), Bai (1981, 1982), Rogers and Shastry (1981), Merzer (1982), Freund et al. (1985), Wright and Walter (1987), Grady and Kipp (1987), Needleman (1989), Shawki and Clifton (1989), Batra and Kim (1991, 1992), Grady (1992), Needleman and Tvergaard (1992), Nemat-Nasser (1992), Shawki (1992), Zhib and Aifantis (1992), Gioia and Ortiz (1996), Kalthoff (1987), Mason et al. (1994), and Zhou et al. (1994, 1996a,b, 1997). On the other hand, microscopic studies have revealed material deformation, damage and failure mechanisms associated with the localization process. For example, Cho et al. (1990, 1993) analyzed the local temperature profiles inside shear bands in several metals. They also found that rotation and alignment of martensitic laths accompany shear band development. The experiments of Andrade et al. (1994) suggested the occurrence of dynamic recrystallization in copper during shear localization. Other microscopic studies have been reported by e.g. Rogers and Shastry (1981), Giovanola (1988), Machand and Duffy (1988), Duffy et al. (1992), Bai et al. (1994), Ramesh (1994), Zurek (1994), Meyers et al. (1995), and Xu et al. (1996).

Grady (1994) derived a shear band toughness measure which is indicative of the amount of energy dissipated in propagating shear bands approximated by a one-dimensional model. This quantity is a function of parameters in a simplified material constitutive model and does not account for microscopic damage and ultimate rupture which leads to the eventual failure of materials inside shear bands. Experiments have indicated that the dynamic shear failure of metals is controlled by ductile damage mechanisms as well as their thermomechanical constitutive behavior. Beatty et al. (1991) showed that 4340 steels with the same hardness value but different carbon distributions absorb varying amounts of energy in a split Hopkinson bar experiment. They also identified the importance of grain size on the susceptibility of copper to shear banding, Andrade et al. (1994). Bai et al. (1994) pointed out that shear band formation in Ti-6Al-4V does not necessarily cause a loss of load-carrying capability. Instead, a loss is observed only after the occurrence of a sudden rupture due to the coalescence of microcracks. Clearly, in order to assess realistically this form of failure, experiments and models accounting for both macroscopic constitutive response and microscopic characterizations are needed.

The objective of this research is to identify, on macro- and microscopic scales, the factors that determine the resistance of materials to dynamic shear failure in the form of shear band formation and eventual rupture and provide an assessment of the

relative resistance to this form of failure. The focus is on both the evolution of the load-carrying capacity of these materials during shear band development and associated microscopic changes. The materials studied are structural metals HY-80, HY-100, HSLA-80, 4340VAR and Ti-6Al-4V. These are the materials for many structures and shear banding is the major mode of failure under certain dynamic loading conditions. For example, Hanchak *et al.* (1993) have demonstrated that shear band formation dominates the dynamic perforation of HY-100 steel. The experiments used in this analysis provide a range of loading rates and superimposed hydrostatic pressures. Deformations can be controlled to occur to various stages of shear local-ization and failure, allowing shear bands to be "frozen" at different levels of straining and analyzed using optical and electron microscopy. The experiments will also allow the evolution of the load-carrying capacity of the materials to be obtained and evaluated. Since a range of materials with different macroscopic properties and micro-structures are analyzed under similar conditions, the results of this research can contribute to the quantification of the "shear band toughness" of materials.

2. MATERIALS

The four structural steels and one titanium alloy studied are listed in Table 1 along with their chemical compositions. HY-80 and HY-100 are carbon steels with different levels of yield strength resulting from their different carbon and magnesium contents. HSLA-80 is a low alloy substitute of HY-80 with a lower amount of carbon and an increased amount of magnesium. The 4340VAR steel is a low alloy steel. Ti-6Al-4V is a high temperature titanium alloy. The heat treatment conditions and the resulting static strength and hardness parameters are shown in Table 2.

The microstructures of the four steels are shown in Fig. 1(a)–(d). The micro-structures of HY-80, HSLA-80 and 4340VAR steels consist of ferrite (light) and pearlite (dark). The size scales for the two constituents vary, with HSLA-80 having the finest phase morphology and 4340 having the coarsest phase morphology. HY-100 has a martensitic microstructure, in contrast to those of the other three steels. This microstructure gives HY-100 a higher static strength than the other steels. The Ti-6Al-4V alloy has a microstructure consisting of equiaxial α-phase (light) and β-phase (dark), as shown in Fig. 2. The α-phase has a volume fraction of approximately 80%. The static strength of the titanium alloy is the highest among the materials analyzed.

3. DYNAMIC SHEAR FAILURE EXPERIMENT

An experimental configuration involving a hat specimen geometry is used. The geometry of the specimen is illustrated in Fig. 3. The specimens are machined from one inch plates, with their axes parallel to the plate normal. This experiment is used to subject the materials to nominal shear deformations in the strain rate range of 10^2–$10^4 \, s^{-1}$. This configuration was first used by Beatty *et al.* (1991), Andrade *et al.* (1994), and Meyers *et al.* (1995) to analyze the shear deformation of a 4340 steel and copper.

Table 1. *Chemical compositions of materials analyzed*

	C	FE	H	MN	P	S	CU	SI	NI	CR	MO	V	TI	AI	CB	SB	AS	SN	O2
HY-80	0.12			0.23	0.014	0.012	0.14	0.21	2.34	1.53	0.25	0.01	0.003			0.005	0.009	0.01	
HY-100	0.16			0.29	0.006	0.002	0.16	0.27	2.38	1.36	0.25	0.006	0.002			0.005	0.006	0.01	
HSLA-80	0.05			0.54	0.004	0.005	1.19	0.25	0.85	0.75	0.22	0.006	0.003	0.018	0.036	0.003			
4340VAR	0.43			0.79	0.005	0.001	0.06	0.31	1.8	0.83	0.26								
Ti-6Al-4V	0.028	0.15	0.0061						0.01			3.985	BAL	6.12					0.17

Table 2. *Heat treatment and quasistatic properties*

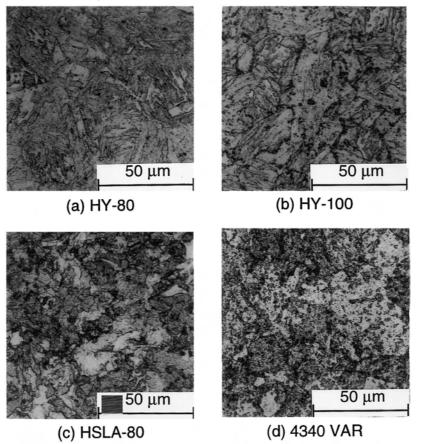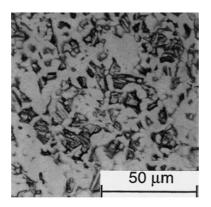|	HY-80	HY-100	HSLA-80	4340 VAR	Ti-6Al-4V
Tensile strength	737 MPa	841 MPa	717 MPa	700 MPa	979 MPa
Yield strength	662 MPa	765 MPa	662 MPa	620 MPa	903 MPa
Hardness	RC 21	RC 28	RC 22	RC 19	RC 36
Heat treatment	1650 F for 70 min, WQ 1240 F for 46 min, WQ	1650 F for 31 min, WQ 1160 F for 98 min, WQ	1650 F for 18 min, WQ 1180 F for 42 min, A/C	1700 F for 60 min, A/C below 600 F 1250 F for 120 min, A/C	Anneal at 1450 F for 8 h

Fig. 1. Microstructures of the steels analyzed; (a) HY-80, (b) HY-100, (c) HLSA-80, and (d) 4340VAR.

Fig. 2. Microstructure of Ti-6Al-4V alloy.
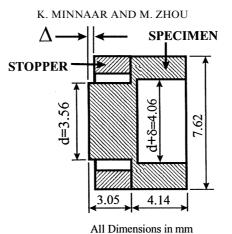
All Dimensions in mm
Fig. 3. A schematic illustration of specimen configuration.

This technique has also been used by Subhash and Ravichandran (1993) in a study of the deformation and failure of hafnium. A split Hopkinson compression bar as described by Follansbee (1985) is used to cause the compressive loading to the specimen along its axis. The specimen geometry is such that upon compressive loading at the two ends, intense shear deformation is obtained in the ligament between the smaller top section and the hollow cylinder section. A stopper ring is placed around the hat during the experiment to control the amount of shear deformation imparted to the ligament. The hat section protrudes above the ring surface and the amount of protrusion (Δ) determines the maximum amount of deformation allowed. Upon loading of the specimen, the hat section deforms until the incident bar touches the ring surface. The relatively small size of the ligament ensures that deformations in the hat and hollow cylinder sections are small and negligible compared to the deformation in the ligament. The maximum average shear strain in the ligament is $\gamma_{\mathrm{max}} = 2\Delta/\delta$. By varying the thickness of the stopper ring, a range of shear deformations can be obtained for each material. After the experiment, the specimens are sectioned in halves and polished. The steels are etched with a 3% nital solution and the titanium is etched with Kroll's solution. The length and width of the shear band are measured on a Reickerd optical microscope. The length of any visible rupture within the shear band is measured. Optical and scanning electron microscopy are used to examine the fracture surfaces for the specimens with completely ruptured ligaments.

4. RESULTS

4.1. *Dynamic constitutive response*

The dynamic constitutive behaviors of the materials are analyzed using the same split Hopkinson compression bar apparatus. The specimen is a cylinder 3 mm in diameter and 3 mm in length. The stress-strain curves for the five materials over the

strain rate range of 10^2–10^4 s^{-1} are shown in Fig. 4(a)–(e). A comparison of the dynamic responses of the materials for similar strain rates between 2.1–2.4 × 10^4 s^{-1} is given in Fig. 4(f). The curves show that like their similar quasistatic yield strengths and ultimate tensile strengths, the steels have similar dynamic constitutive behaviors in the strain rate range of 10^2–10^4 s^{-1}. The similar quasistatic and dynamic responses indicate that the steels have nearly the same rate-sensitivities in the strain rate range analyzed. It can be seen in Fig. 4(f) that the steels also have nearly the same rate of strain hardening.

Ti-6Al-4V has a much stronger rate-sensitivity than those of the steels. In addition, its rate of strain hardening is slightly higher. Despite these factors, this material is more susceptible to shear banding and ductile rupture than the steels, as suggested by the precipitous drops in stress at strains of approximately 0.2. Postmortem analysis revealed that the shear bands occurred along plane approximately 45° from the loading axis. This is inconsistent with the understanding that strong rate-sensitivity and higher strain hardening enhance resistance to shear localization, indicating factors other than rate-sensitivity play a more dominant role in determining shear failure under the conditions analyzed. Further discussions on this will follow in later sections. Shear bands are not observed for the steels in uniaxial compression experiments.

4.2. *Evolution of stress-carrying capacity throughout deformation and failure*

The nominal shear stress-strain curves obtained from shear failure experiments for all five materials are shown in Fig. 5(a)–(e). The stress and strain are average values in the specimen ligament. The shear stress is obtained by dividing the total load applied to the specimen by the cylindrical surface area in the ligament. The shear strain is obtained via

$$\gamma = \frac{2u(t)}{\delta},$$

where $u(t)$ is the decrease in the length of the hat specimen. This calculation assumes that all the deformation occurs in the ligament. For each material, results for several stopper thickness values are shown. The precipitous drops in shear stress signifies the loss of stress-carrying capacity associated with shear failure development. The increase in stress following the drop on each curve results from the contact of the incident bar and the stopper. It does not represent material behavior. Rather, it signifies the cessation of deformation in the specimen. To facilitate comparison, the curves for all five materials for the stopper thickness allowing complete failure are shown in Fig. 5(f). Clearly, all materials show a total loss of stress-carrying capacity indicated by the drop of stress to near zero levels. The shape of the curves indicate that the strains at which materials lose all of their stress-carrying capacities increase in the order Ti-6Al-4V → HY-80 → HY-100 → HSLA-80 → 4340VAR. The critical strain level for Ti-6Al-4V is approximately 1.6—significantly lower than those of the steels. Ti-6Al-4V does not display a period of gradual decrease of stress. Instead, a rapid loss of stress is observed immediately after the onset of localization. The steels, on the other hand, show gradual softening preceding the rapid losses of load-carrying capacity, indicating higher resistance to shear failure.
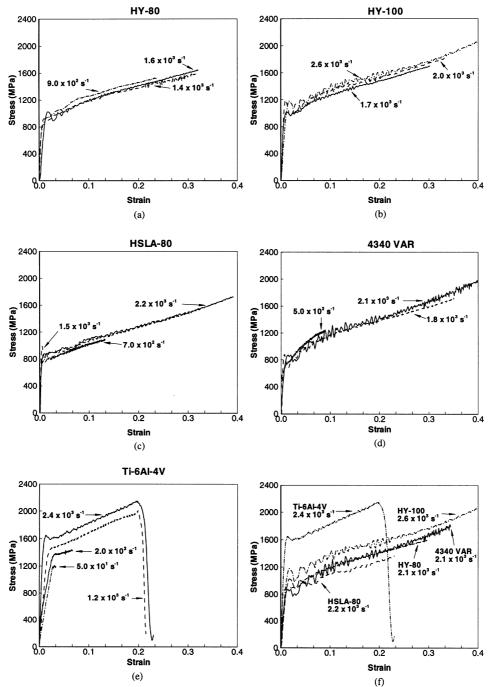
Fig. 4. Constitutive response over a range of strain rates for (a) HY-80, (b) HY-100, (c) HSLA-80, (d) 4340VAR, (e) Ti-6Al-4V alloy ; (f) is a comparison of all materials at similar rates.
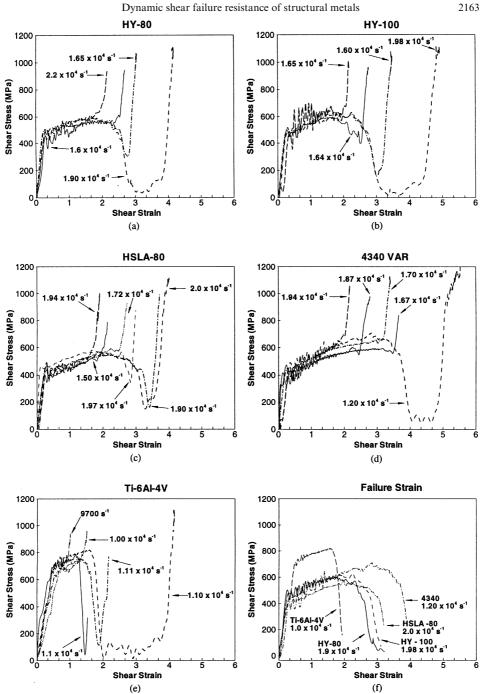
Fig. 5. Nominal stress-strain curves during shear deformation and failure for; (a) HY-80, (b) HY-100, (c) HSLA-80, (d) 4340VAR, (e) Ti-6Al-4V alloy, and (f) a comparison of all materials deformed until complete failure occurs.

4.3. *Microscopic observations*

To compare microstructural evolution during the shear failure process, the deformed microstructures of the steels at nominal shear strain levels of 2.0 and 2.5 are shown in Fig. 6. This series of pictures illustrates the progression of localization and rupture in each material. HY-100 shows distinct shear band formation across the whole ligament of the specimen at $\gamma = 2.0$. The band is narrow (~ 60–70 μm in width) compared with those in the other steels. At $\gamma = 2.5$, complete rupture has occurred along the shear band. This material shows the most extensive microscopic damage among the steels. For HY-80, a shear band is emerging from one side of the ligament at $\gamma = 2.0$. The band has propagated through the ligament at $\gamma = 2.5$ but no crack is seen. Note that the notch on the right hand corner is formed by the motion of the initial free surfaces and does not represent a crack. SEM photographs of the ruptured specimens indicate that the original radius of the specimen folds inward as the shear deformation increases. This folded surface is noticeable in all the specimens in which the shear band has not completely propagated across the ligament. A shear band is emerging from one side of the ligament at $\gamma = 2.0$. The localization of deformation in 4340VAR occurs later than in all other steels. In addition, the deformation is diffuse and the shear band has a width of approximately 260 μm, 3–4 times those in HY-80, HY-100 and HSLA-80. The increasing order of shear failure resistance for the steels appears to be HY-100 $\rightarrow$ HY-80 $\rightarrow$ HLSA-80 $\rightarrow$ 4340. This is different from the order of decreasing critical shear strain indicating the onset of loss of stress-carrying capacity seen in Fig. 5. It seems that the martensitic microstructure of HY-100 makes it more susceptible to the development of intensely localized shear bands. However, its earlier development of localization does not necessarily result in early loss of stress. Rather, significant loss of strength follows more closely the subsequent ductile rupture of materials. This observation is consistent with what was reported by Bai *et al.* (1994).

The deformed microstructures of Ti-6Al-4V at $\gamma = 1.3$ and 2.0 are shown in Fig. 7. Note that the strains here are from those in Fig. 6, indicating shear failure occurs significantly earlier in the titanium alloy than in the steels. The shear band in this material has a width of only 10 μm (Fig. 8), nearly an order of magnitude smaller than those in the steels. In addition to the extremely intense shear deformation, the shear band is closely followed by cracks formed through the microrupture of damaged materials inside the shear band, Fig. 8. Note that while no shear band is seen in Fig. 7(a) at $\gamma = 1.3$, nearly complete fracture has occurred in Fig. 7(b) at $\gamma = 2.0$, indicating the full development of localization and rupture in this material is within a nominal shear strain increment of 0.41. This rapid occurrence of failure has been observed in the stress-strain profiles for this material in Fig. 5(e).

To quantify the extent of shear localization and rupture, the lengths of shear bands and cracks following the shear bands are measured and plotted in Fig. 9. These two lengths increase with the nominal shear strain inside the ligament. For each of the steels, there is an appreciable difference in the shear band length and the crack length, suggesting development of rupture after localization of strain. For Ti-6Al-4V, the shear band length and the rupture length are very close to each other. This lack of difference for the titanium alloy indicates the near simultaneous occurrence of localization and rupture.

γ=2.0 γ=2.5

(a) HY-80
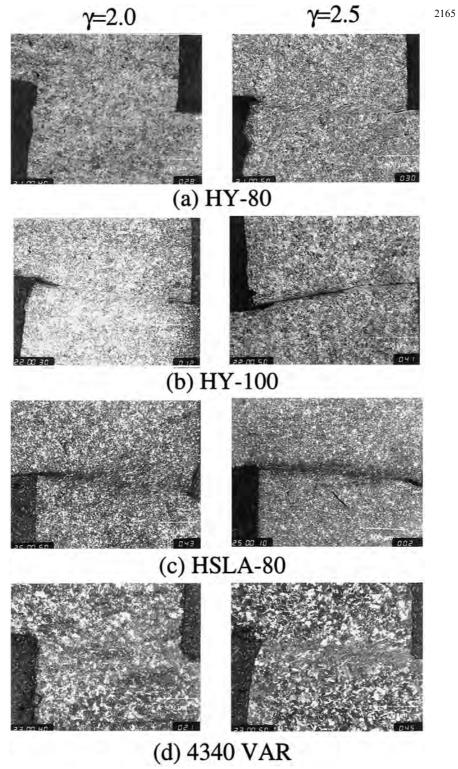
(b) HY-100

(c) HSLA-80

(d) 4340 VAR

Fig. 6. Morphologies of shear bands and ductile rupture at $\gamma = 2.0$ and 2.5 for (a) HY-80, (b) HY-100, (c) HSLA-80, (d) 4340VAR.
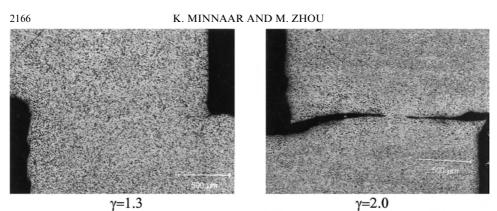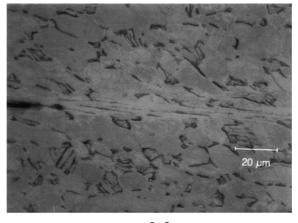
Fig. 7. Morphologies of shear bands and ductile rupture at $\gamma = 1.3$ and 2.0 for Ti-6Al-4V.

Fig. 8. A close up look of the shear band in Ti-6Al-4V at $\gamma = 2.0$.

Partly because of this rapid development of rupture, Ti-6Al-4V exhibits a much higher degree of susceptibility to the loss of stress-carrying capacity than those of the steels.

5.   DISCUSSION AND SUMMARY

Although it is based on an approximate characterization of the thermomechanical response and a one-dimensional deformation model, the shear band dissipation energy derived by Grady (1994) allows the energy dissipated per unit area of shear band growth for different materials to be estimated and compared. This shear band dissipation energy is
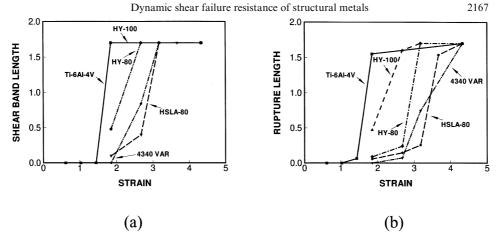
Fig. 9. Shear band and rupture lengths as a function of shear deformation; (a) shear band length, (b) rupture length.

Table 3. *Dissipation energy and shear band toughness*

Material	Flow stress (MPa)	Dissipation energy Γ_s (KJ/m²)	Shear band toughness K_s (MPa$\sqrt{m}$)
HY-80	1460	125.2	142.221
HY-100	1530	120.9	139.745
HSLA-80	1280	138.2	149.414
4340VAR	1450	125.9	142.588
Ti-6Al-4V	2000	3.935	18.861

$$\Gamma_s = \frac{\rho c}{\alpha} \left(\frac{9\rho^3 c^2 \chi^3}{\tau_y^3 \alpha^2 \dot{\gamma}} \right)^{1/4}$$

where ρ is density, χ is thermal diffusion coefficient, α is a thermal softening coefficient, c is specific heat, τ_y is the flow stress at strain rate $\dot{\gamma}$. This parameter is calculated for the materials analyzed in the experiments. For the steels, their densities, thermal diffusion coefficients, and thermal softening coefficients are similar (due to similar melting points) and are taken as $\rho = 7.85 \times 10^3$ kg m^{-3}, $\alpha = 6.5 \times 10^{-4}$ m^2 s^{-1}, and $c = 503$ J·(kg·K)$^{-1}$, respectively. For Ti-6Al-4V, these parameters are $\rho = 4.43 \times 10^3$ kg m^{-3}, $\alpha = 5.6 \times 10^{-4}$ m^2 s^{-1}, and $c = 526$ J·(kg·K)$^{-1}$. The flow stress τ_y for each material is taken from its stress strain curves in Fig. 4 at a strain rate of $\dot{\gamma} = 1.7 \times 10^4$ s^{-1}. The values are listed in Table 3 along with the values of calculated Γ_s. A shear band toughness parameter is defined by Grady as $K_s = \sqrt{2G\Gamma_s}$, where G is the shear modulus. It can be seen that the dissipation energy and shear band toughness values for the steels are very close to each other due to their similar thermal and mechanical properties. This similarity is in contrast to the significantly different shear failure

behaviors observed in the experiments. In addition to the approximate nature of the model on which the calculation of Γ_s is based, the lack of agreement between the values of these quantities and the shear failure resistance of the materials observed has to do with the influence of microscopic damage not accounted for in the analysis.

The shear stress-shear strain curves obtained in the experiments described above and the microscopic observations assign mostly consistent shear failure toughness rankings for the materials analyzed. From the most susceptible to the least susceptible, the ranking is Ti-6Al-4V, HY-80, HY-100, HSLA-80, 4340VAR based on the stress-strain curves or Ti-6Al-4V, HY-100, HY-80, HSLA-80, 4340VAR based on the microscopic morphologies of shear bands and fracture behind the shear band tips. The stress-strain response and the microscopic analysis showed that Ti-6Al-4V is more susceptible to dynamic shear failure than the steels considered. This is in contrast to its much higher rate sensitivity than those of the steels. Similarly, among the steels, significant difference in the shear failure behavior is observed, despite their similar thermal and mechanical constitutive behavior over the strain rate range of 10^2–10^4 s^{-1}. The discrepancies can be partly attributed to the fact that the formation of a well-deformed shear band does not necessarily cause an instantaneous loss in load carrying capability. The subsequent coalescence of cracks or development of rupture also plays a significant role in determining the evolution of the load-carrying capacity of materials during shear deformation. Clearly, microscopic damage as well as the thermal-mechanical response of materials needs to be considered in evaluating the dynamic shear failure resistance of materials.

The calculated dissipation energy value for Ti-6Al-4V and the calculated shear band toughness value are only fractions of those for the steels. This partly explains its much higher susceptibility to shear failure compared with those of the steels and demonstrates that thermomechanical behavior plays a very important role in determining material shear failure resistance. However, the experiments showed that rupture closely follows the propagating shear bands in this material, further expediting the progression of failure through rapid release of stress. Like in the case of the steels, this effect should not be neglected. A comparison of the microscopic rupture mechanism in the form of void growth and coalescence in these materials is being carried out using scanning electron microscopy. The result and its implications for the shear failure resistance of these materials will be reported in a future publication.

ACKNOWLEDGEMENTS

REFERENCES

Andrade, U., Meyers, M. A., Vecchio, K. S. and Chokshi, A. H. (1994) Dynamic recrystallization in high-strain, high-strain-rate plastic deformation of copper. *Acta Metall. Mater.* **42**, 3183–3195.

Bai, Y. L. (1981) A criterion for thermo-plastic shear instability. Proceedings of the Inter-

national Conference on Metallurgical Effects of High-Strain-Rates Deformation and Fabrication, Albuquerque, NM, Plenum, NY, 277–283.

Bai, Y. L. (1982) Thermo-plastic instability in simple shear. *J. Mech. Phys. Solids* **30,** 195–207.

Bai, Y., Xue, Q., Xu, Y. and Shen, L. (1994) Characteristics and microstructure in the evolution of shear localization in Ti-6Al-4V alloy. *Mech. Mater.* **17,** 155–164.

Batra, R. C. and Kim, C. H. (1992) Analysis of shear banding in twelve materials. *Int. J. Plasticity* **8,** 425–452.

Batra, R. C. and Kim, C. H. (1991) Effect of thermal conductivity on the initiation, growth and band width of adiabatic shear bands. *Int. J. Engng Sci.* **29,** 949–960.

Beatty, J. H., Meyer, L. W., Meyers, M. A. and Nemat-Nasser, S. (1991) Formation of controlled adiabatic shear bands in AISI 4340 high strength steel. *12th Army Symposium on Solid Mechanics*, Plymouth, MA.

Cho, K., Chi, Y. C. and Duffy, J. (1990) Microscopic observations of adiabatic shear bands in three different steels. *Metall. Trans. A.* **21A,** 1161–1175.

Cho, K., Lee, S., Nutt, S. R. and Duffy, J. (1993) Adiabatic shear band formation during dynamic torsional deformation of an HY-100 steel. *Acta Metall. Mater.* **41,** 923–932.

Clifton, R. J. (1980) Adiabatic shear banding. *Material Response to Ultra-High Loading Rates*, NMAB-356, National Materials Advisory Board (NRC), Washington, D.C., Chap. 8.

Duffy, J. and Chi, Y. C. (1992) On the measurement of local strain and temperature during the formation of adiabatic shear bands. *Mat. Sci. Engng* **A157,** 195–210.

Follansbee, P. S. (1985) The hopkinson bar, *Metals Handbook*, **8,** American Society for Metals, Metals Park, Ohio, 198–217.

Freund, L. B., Wu, F. H. and Toulios, M. (1985) *Proc. Considere Memorial Symposium*. Presse de l'Ecole Nationale des Pontes et Chaussees, Paris, France, p. 125.

Gioia, G. and Ortiz, M. (1996) The two-dimensional structure of dynamic shear bands in thermoviscoplastic solids. *J. Mech. Phys. Solids* **44,** 251–292.

Giovanola, J. H. (1988) Adiabatic shear banding under pure shear loading, Part I : Direct observation of strain localization and energy dissipation measurements ; Part II : Fractographic and metallurgraphic observations. *Mech. Mater.* **7,** 59–87.

Grady, D. E. (1992) Properties of an adiabatic shear-band process zone. *J. Mech. Phys. Solids* **40,** 1197–1215.

Grady, D. E. (1994) Dissipation in adiabatic shear bands. *Mech. Mater.* **17,** 289–293.

Grady, D. E. and Kipp, M. E. (1987) The growth of unstable thermoplastic shear with application to steady-wave shock compression in solids. *J. Mech. Phys. Solids* **35,** 95–118.

Hanchak, S. J., Altman, B. S. and Forrestal, M. J. (1993) Perforation of HY-100 steel plates with long rod projectiles. *Proceedings of the* 13*th Army Symposium on Solid Mechanics*, Plymouth, MA, pp. 247–257.

Kalthoff, J. F. (1987) Shadow optical analysis of dynamic shear fracture. *SPIE* **814,** Photomechanics and Speckle Metrology, 531–538.

Marchand, A. and Duffy, J. (1988) An experimental study of the formation process of adiabatic shear bands in a structural steel. *J. Mech. Phys. Solids* **36,** 251–283.

Mason, J. J., Rosakis, A. J. and Ravichandran, G. (1994) Full field measurements of the dynamic deformation field around a growing adiabatic shear band at the tip of a dynamically loaded crack or notch. *J. Mech. Phys. Solids* **42,** 1679–1697.

Merzer, A. M. (1982) Modelling of adiabatic shear band development from small imperfections. *J. Mech. Phys. Solids* **30,** 323–338.

Meyers, M. A., Andrade, U.R. and Chokshi, A. H. (1995) The effect of grain size on the high-strain, high-strain-rate behavior of copper. *Metall. & Meater. Trans. A.* **26A,** 2881–2893.

Molinari, A. and Clifton, R. J. (1987) Analytical characterization of shear localization in thermoviscoplastic materials, Trans. of ASME. *J. Appl. Mech.* **54,** 806–812.

Needleman, A. (1989) Dynamic shear band development in plane strain. *J. Appl. Mech.* **56,** 1–9.

Needleman, A. and Tvergaard, V. (1992) Analysis of plastic flow localization in metals. *Appl. Mech. Rev.* **45**(Suppl.), S3-S15.

Nemat-Nasser, S. (1992) Phenomenological theories of elastoplasticity and strain localization at high strain rates. *Appl. Mech. Rev.* **45**(Suppl.), S19–S45.

Ramesh, K. T. (1994) On the localization of shearing deformations in a tungsten heavy alloy. *Mech. Mater.* **17,** 165.

Rogers, H .C. (1979) Adiabatic plastic deformation. *Ann. Rev. Mat. Sci.* **9,** 283–311.

Rogers, H. C. and Shastry, C. V. (1981) Material factors in adiabatic shearing in steels. *Shock Waves and High Strain-rate Phenomena*, ed. M. A. Meyers and L. E. Murr, Chap. 18, pp. 285–298. Plenum Press.

Shawki, T. G. (1992) The phenomenon of shear strain localization in dynamic viscoplasticity. *Appl. Mech. Rev.* **45,** S46–S60.

Shawki, T. G. and Clifton, R. J. (1989) Shear band formation in thermal viscoplastic materials. *Mech. Mat.* **8,** 13–43.

Subhash, G. and Ravichandran, G. (1993) High strain rate behavior and localization in hafnium. *Experimental Techniques in the Dynamics of Deformable Solids*, ed. K. T. Ramesh, AMD-Vol. 165, pp. 79–88. ASME.

Wright, T. W. and Walter, J. W. (1987) On stress collapse in adiabatic shear bands. *J. Mech. Phys. Solids* **35,** 701–720.

Xu, Y. B., Bai, Y. L., Xue, Q. and Shen, L. T. (1996) Formation, microstructure and development of the localized shear deformation in low-carbon steels. *Acta Mater.* **44,** 1917–1926.

Zbib, H. M. and Aifantis, E. C. (1992) On the gradient-dependent theory of plasticity and shear banding. *Acta Mechanica* **92,** 209–255.

Zhou, M., Needleman, A. and Clifton, R. J. (1994) Finite element simulations of dynamic shear localization in plate impact. *J. Mech. Phys. Solids* **42,** 423–458.

Zhou, M., Rosakis, A. J. and Ravichandran, G. (1996(a)) Dynamically propagating shear bands in impact-loaded prenotched plates, I—Experimental investigations of temperature signatures and propagation speed. *J. Mech. Phys. Solids* **44,** 981–1006.

Zhou, M., Ravichandran, G. and Rosakis, A. J. (1996(b)) Dynamically propagating shear bands in impact-loading prenotched plates, II—Numerical simulations. *J. Mech. Phys. Solids* **44,** 1007–1032.

Zhou, M. and Clifton, R. J. (1997) Dynamic constitutive and failure behavior of a two-phase tungsten composite. *J. App. Mech.* **64,** 487–494.

Zurek, A. K. (1994) The study of adiabatic shear band instability in a pearlitic 4340 steel using a dynamic punch test. *Metall. & Mater. Trans. A.* **25A,** 2483–2489.